Two-dimensional ionization chamber arrays for IMRT plan verification

Bjoern Poppe[a)]
Klinik fuer Strahlentherapie und Internistische Onkologie, Pius-Hospital, Oldenburg, Germany, and Carl-von-Ossietzky-Universitaet Oldenburg, Oldenburg, Germany

Arne Blechschmidt and Armand Djouguela
Carl-von-Ossietzky-Universitaet Oldenburg, Oldenburg, Germany

Ralf Kollhoff, Antje Rubach, and Kay C. Willborn
Klinik fuer Strahlentherapie und Internistische Onkologie, Pius-Hospital, Oldenburg, Germany

Dietrich Harder
Georg-August-Universitaet Goettingen, Goettingen, Germany

(Received 13 August 2004; revised 1 February 2006; accepted for publication 1 February 2006; published 22 March 2006)

In this paper we describe a concept for dosimetric treatment plan verification using two-dimensional ionization chamber arrays. Two different versions of the 2D-ARRAY (PTW-Freiburg, Germany) will be presented, a matrix of 16×16 chambers (chamber cross section 8 mm $\times$ 8 mm; the distance between chamber centers, 16 mm) and a matrix of 27×27 chambers (chamber cross section 5 mm $\times$ 5 mm; the distance between chamber centers is 10 mm). The two-dimensional response function of a single chamber is experimentally determined by scanning it with a slit beam. For dosimetric plan verification, the expected two-dimensional distribution of the array signals is calculated via convolution of the planned dose distribution, obtained from the treatment planning system, with the two-dimensional response function of a single chamber. By comparing the measured two-dimensional distribution of the array signals with the expected one, a distribution of deviations is obtained that can be subjected to verification criteria, such as the gamma index criterion. As an example, this verification method is discussed for one sequence of an IMRT plan. The error detection capability is demonstrated in a case study. Both versions of two-dimensional ionization chamber arrays, together with the developed treatment plan verification strategy, have been found to provide a suitable and easy-to-handle quality assurance instrument for IMRT. [DOI: 10.1118/1.2179167]

Key words: 2D-ARRAY, IMRT, dose plan verification

I. INTRODUCTION

Highly conformal radiation treatments involving intensity-modulated photon fields have increasingly been applied in recent years.[1–6] The goal of these techniques is to achieve dose distributions of increased conformity to the target volumes, while further reducing the doses to nontarget organs at risk. Reducing the side effects to these organs permits the escalation of the tumor dose and a better tumor control. Often this can only be achieved by increasing the dose inhomogeneity.[5] Such dose distributions can be created by segmental techniques (SMLC, or step-and-shoot), dynamic techniques (DMLC) and the application of absorbers. Since these techniques provide strongly modulated dose profiles, great care must be taken to ensure their correct application. Along with improved patient immobilization accuracy, many machine- and system-dependent parameters must be analyzed and carefully adjusted before starting intensity-modulated radiation therapy (IMRT).

In this framework, the dosimetric verification of treatment plans is one of the major tasks under investigation. Film dosimetry has become the most important technique to verify two-dimensional dose distributions.[7–10] Other methods such as gel dosimetry[11,12] and portal imaging[13] have not gained broad acceptance due to high costs and complicated applications. A cost-effective and easy-to-handle instrument is provided by two-dimensional detector arrays. Using shielded *n*-type silicon diodes, detector arrays have been developed that monitor doses at predefined regions within the radiation field.[14–16] A semiconductor detector array has also been devised for in-phantom dosimetry.[17] Air-filled detectors have been used in a pixel-segmented ionization chamber,[18] and a further approach has been by a scintillation detector plate viewed by a CCD camera.[16]

Together with PTW-Freiburg, we have developed two-dimensional ionization chamber arrays known as the PTW 2D-ARRAYs. Version 1 is equipped with 256 independent ionization chambers, whereas version 2 comprises 729 chambers.[19–22] Spezi *et al.*[23] and Wiezorek *et al.*[16] recently investigated various dosimetric properties of version 2. In this paper we will describe some basic properties of both versions of the 2D-ARRAYs, particularly the two-dimensional response functions of a single chamber, and the procedures underlying the application of both versions for IMRT plan verification.

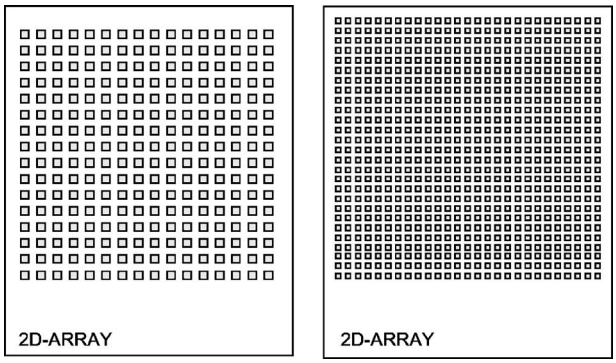

FIG. 1. Schematic drawings of the 2D-ARRAYs commercially available. Left: version 1 (PTW type 10017), 16×16 ionization chambers. Right: version 2 (PTW type 10024), 27×27 chambers.

II. MATERIALS AND METHODS

A. Linear accelerators

All measurements have been performed using linear accelerators with nominal acceleration voltages of 6, 10, and 15 MV (Siemens Primus, Siemens Digital-Mevatron, Siemens Medical Systems, Concord, CA). In our linear accelerators, the beam pulse duration is 3 μs and the pulse repetition time is 6.1 ms for the dose rate usually applied in IMRT (6 MV, 200 MU/min). The accelerators were equipped with multileaf collimators with a leaf width, projected onto the isocenter plane, of 1 cm. In studies of the detectability of leaf position errors, several MLC leaves were misaligned by introducing an error into the leaf data file of the Record & Verify system.

B. 2D-ARRAY

The 2D-ARRAY (PTW-Freiburg, Germany) is available in two versions that provide different numbers and sizes of ionization chambers. Version 1 (PTW type 10017) consists of 256 air-filled ionization chambers arranged in a 16×16 matrix, covering an area of 27 cm×27 cm (Fig. 1). Each single chamber has a cross section of 8 mm×8 mm and an air-filled volume height of 5 mm. Ridges of low-Z material, each 8 mm wide, separate the ionization chambers from one another. The chambers lie in one common plane, and the ridges prevent laterally scattered secondary electrons from drifting across more than one chamber. The centers of adjacent chambers are placed at distances of 16 mm from each other. Version 2 (PTW type 10024) consists of 729 air-filled ionization chambers arranged in a 27×27 matrix covering an area of 27 cm×27 cm (Fig. 1). Each single chamber has a cross section of 5 mm×5 mm and an air-filled volume height of 5 mm. The chambers are separated from each other by 5 mm. The distance between the centers of adjacent chambers is 10 mm, which is equal to the width of one leaf pair of the most common multileafcollimators (MLCs), projected into the isocenter plane. This permits the projection of each pair of opposing collimator leaves exactly upon one row of chambers, whereby a clear association of the measured readings of this row to a single leaf pair can be achieved. The entrance plane of the 2D-ARRAY is usually arranged perpendicular to the beam's central axis.

Both versions of the 2D-ARRAY are operated at a chamber voltage of 400 V. The 2D-ARRAY accumulates the collected electrical charge of each chamber on a capacitor, which is read out and reset every 400 ms. The reset logic works without dead time, and after the capacitor has been reset, the further increment of the collected charge is recorded without loss. In both versions of the 2D-ARRAY, the air-filled ionization chambers are covered with a 5 mm thick PMMA front plate that is a fixed part of the construction. By comparing depth dose curves measured with the arrays and with cylindrical ionization chambers, the effective depth of measurement has been found to be located at the back surface of the 5 mm thick PMMA front plate, i.e., in the entrance plane of the air-filled chamber volumes. The resulting water-equivalent depth is therefore 5.9 mm. Individual chamber calibration is performed by the manufacturer and can be verified with appropriate software, such as MatrixCal (PTW-Freiburg, Germany).

For a 2D-ARRAY version 2, Spezi *et al.*[23] have already demonstrated an excellent short-time reproducibility of ±0.2%. The long-time reproducibility was found to be within ±1% over a period of 4 months. The linearity error, compared with that of an ionization chamber over a dose range from 2 to 500 MU, was smaller than 0.4%. Response deviations from chamber to chamber exceeding the manufacturer's limit of 1% were not observed over a period of several months. Measured output factors[16,23] showed good agreement with ionization chamber measurements for field sizes between 2 cm×2 cm and 27 cm×27 cm.

C. Slit measurements

The entrance plane of the air-filled volumes of the single chambers determines the effective depth of measurement, and each of these volumes will be traversed by secondary electrons emitted from various points in this plane. Due to the ranges of these high-energy electrons, these source points are not only located immediately in front of the air-filled volumes; the volumes will also be traversed by electrons emerging from the ridges between the single chambers. Therefore, each single chamber will have a lateral response function with regard to the secondary electron fluence profile in this plane, and this function is expected to have non-negligible values for points above the ridges.

The lateral response function of a single chamber of the 2D-ARRAY has been investigated using stepwise scanning of a narrow, slit-shaped photon beam across the chamber (Fig. 2). The block collimator jaws were opened to give a nominal beam width of 0.5 mm in the y direction, and the central pair of MLC leaves was opened to define a slit beam length of 8 cm in the x direction. In addition, a pair of cast-metal blocks forming a slightly diverging slit 2.2 mm wide at the entrance side was arranged in the accessory holder and was aligned with the slit beam. The purpose of the tertiary collimator was to absorb photons scattered at the edges of the block collimators and the MLC. The full width at half-

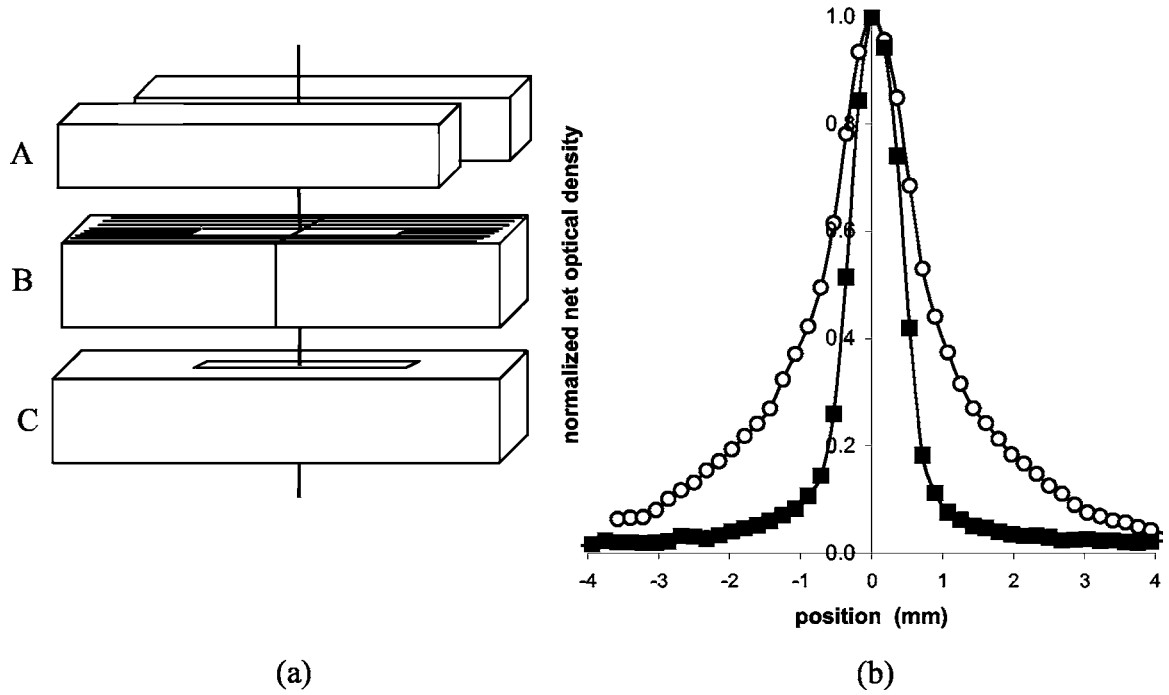

FIG. 2. (a) Scheme of the collimation of a slit beam that had a full half-width of 0.9 mm in the ISO plane. A: Upper collimator, slit width corresponding to 0.5 mm in the ISO plane. B: Lower collimator (MLC), one leaf pair opening with a slit length of 8 cm in the ISO plane. C: Tertiary collimator (cast metal), positioned in the accessory holder, slit width 2.2 mm. (b) Profile of the slit beam (6 MV) in the ISO plane, measured by film dosimetry. Squares: film placed on top of a PMMA phantom, no preabsorber. Circles: film at 5 cm depth in PMMA.

maximum of the slit beam thereby actually realized at 100 cm focal distance, verified by film dosimetry,[10] was 0.9 mm (see Fig. 2). To scan a single chamber with the slit beam, the 2D-ARRAY was placed on a mechanical device that shifted it in steps of 1 mm across the slit beam. The distance between the surface of the array and the lower edge of the cast-metal block was 20 cm.

The whole procedure was repeated after the slit of the tertiary collimator had been closed with a cast-metal block of the same thickness as the tertiary collimator. For each scanning position, the background signal obtained was subtracted from the signal obtained with the open tertiary collimator slit. The difference profile was used to characterize the sensitivity of the ionization chamber.

D. Dosimetry equipment

For reference, a cylindrical ionization chamber, the "pinpoint" chamber with 0.1 cm^3 air volume (PTW M 23332), was used. As recommended by national and international standards, the long-time reproducibility of dose measurements in our clinic is guaranteed by a commercially available radioactive stability check device (PTW T48002). Film dosimetry was applied to investigate the profile of the slit beam[10] and to verify the dose distributions obtained with the 2D-ARRAYs. Kodak EDR2 film (Kodak Inc., Rochester, NY) was used in combination with a film scanner (VIDAR VXR-16 DosimetryPro, VIDAR Systems Corp., Herndon, VA). All phantom measurements were carried out in RW3, a water-equivalent solid material available in the form of plates with a 30×30 cm^2 surface and 1 cm thickness.[24]

E. Treatment planning system

Calculations have been carried out using the treatment planning system Helax 6.1 A (Nucletron, Venendaal, Netherlands). For IMRT, the base data of the treatment planning system (TPS) had been commissioned with ionization chambers, energy-compensated diodes and film dosimetry. According to Dempsey *et al.*,[25] we set the dose grid resolution to 2 mm in order to perform accurate IMRT dose plan calculations. For the later described convolution algorithm of the dose plan values with the lateral response function of a single array chamber, the dose grid was further binned by linear interpolation to a 1 mm grid distance. The Helax TPS system was complemented by a house-made Record & Verify system termed Herbie.[26]

III. RESULTS

A. Dosimetric properties of 2D-ARRAYS

Inside an IMRT field, the instantaneous dose per pulse may vary by a factor of 330. It is therefore important to analyze the dose-per-pulse behavior of the measurement device.[15] The dose per pulse at the isocenter, measured by our standard dosimetry setup (10 cm $\times$ 10 cm field size at a 100 cm focal distance, 15 cm thick water-equivalent phantom RW3[24] at a 90 cm source-to-surface distance, a depth of measurement of 10 cm, 124 MU/Gy) is 1.64×10^{-4} Gy/pulse. According to Boag's theory[28] this corresponds to a collection efficiency for a single ionization chamber of 99.3%. We also compared the signal of an array chamber with that of an ionization chamber (PTW M 23332)

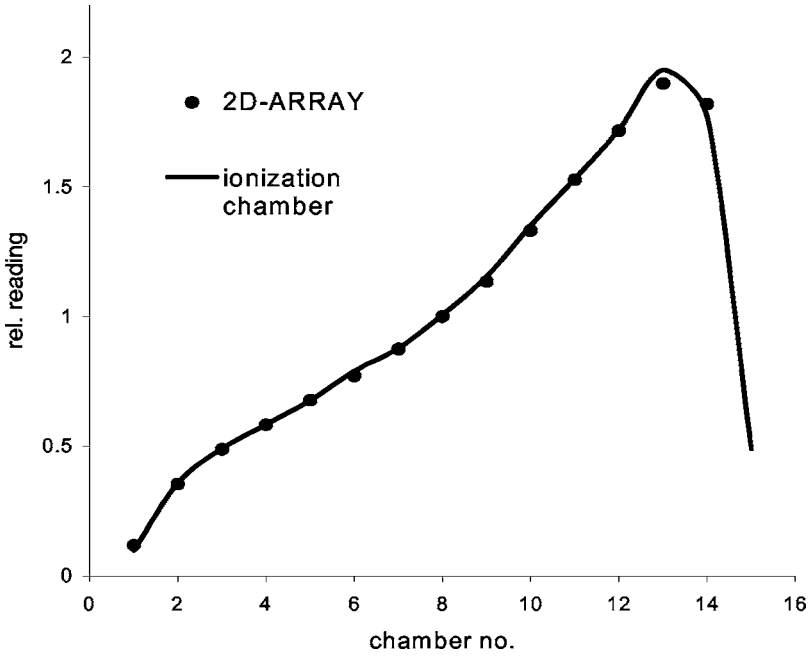

FIG. 3. A comparison of a measured and planned Virtual Wedge profile (60°, 6 MV). Points: 2D-ARRAY (version 2); line: Dose profile measured with ionization chamber.

at various doses per pulse, which were achieved with the help of cast-metal absorber plates arranged in the accessory holder. Over the whole investigated range of doses per pulse, from 1.64×10^{-4} Gy/pulse down to 0.5% of that value, the quotient of the signal of an array chamber and that of the standard ionization chamber did not vary by more than ±0.4%.

The resolution of the digital dose display for each chamber is 1 mGy. In order to illustrate that the correctness of dose measurement is not affected by the leaf speed in dynamic techniques, Fig. 3 shows the comparison of a measured dose profile of a virtual wedge, with jaw movement of approximately 2 cm/s in the isocenter plane, by measurements with the 2D-ARRAY version 2.

Figure 4 shows the field-size-dependent output factor curve of the central chamber of the 2D-ARRAY version 2 compared to that of the "pinpoint" ionization chamber (PTW M 23332) and of an energy-compensated diode (PTW TM 60008) for 6 MV photons. For field sizes below 2 cm $\times$2 cm, the diode represents the correct values, whereas the ionization chambers, due to the volume effect,[27] tend to underestimate the true output factor. Equivalent results have been obtained with 10 and 15 MV photons. At field sizes exceeding 2 cm $\times$ 2 cm, the deviations between the version 2 array (type 10024) and the reference values are less than 1%. The version 1 array (type 10017) shows a deviation smaller than 1% at field sizes exceeding 3 cm $\times$ 3 cm. In view of the good agreement observed between the output factor curves of the ionization chamber and the 2D-ARRAYs for the large fields, it can be concluded that the sensitivity of the array chambers does not have any increased energy dependence that could increase their response to scattered photons, and that the 2D-ARRAY itself has scatter properties close to those of water.

B. Slit measurements of the lateral response function of a single chamber

Measured one-dimensional signal profiles for both arrays obtained by scanning a slit beam are shown in Fig. 5. The background already subtracted in this figure was smaller than 0.5% of the maximum value. The signal profile has a central

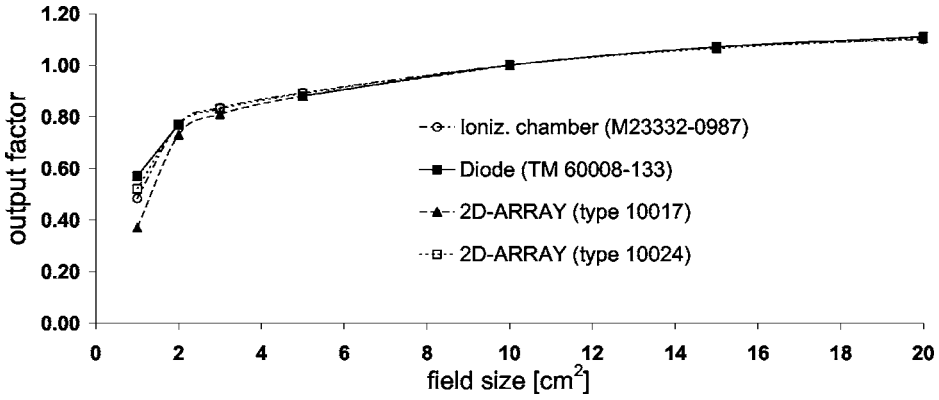

FIG. 4. Field-size-dependent output factors for 6 MV photon radiation, measured with different detectors at a depth of 10 cm in a RW3 phantom (source-to-surface distance 90 cm, 5 cm backscatter material). At the small field sizes, the volume effect of the ionization chambers is clearly detectable.

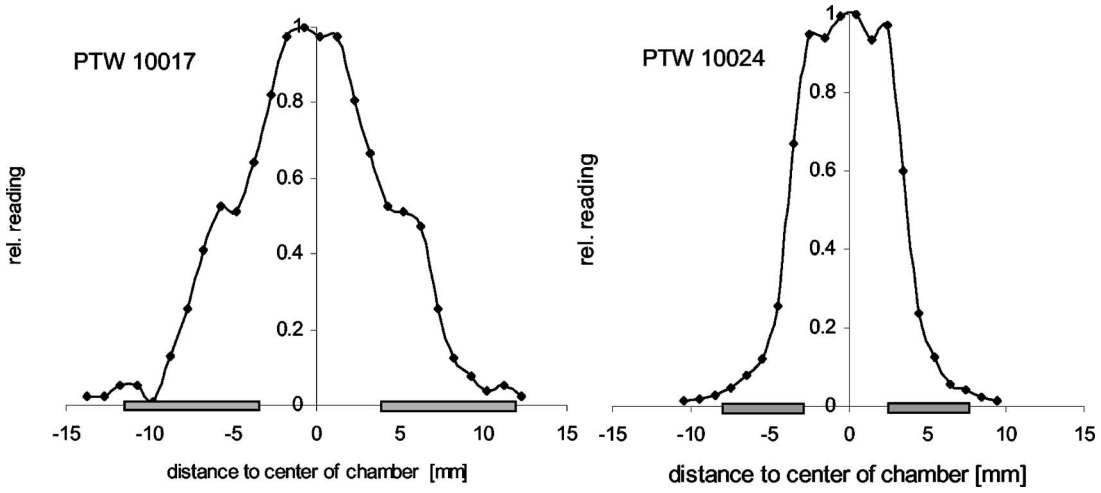

FIG. 5. Lateral response functions of types 1 and 2 of 2D-ARRAYs measured by slit scanning with a slit of 0.9 mm half-width. The gray areas denote the positions of the ridges between two adjacent chambers.

peak accompanied by side peaks corresponding to the inner surfaces of the ridges between the chambers. This shows that photons hitting a ridge are causing a signal due to the transmission into the chamber volume of secondary electrons starting within the ridge. Figure 5 also demonstrates that the response of a single chamber is less than 6% (type 1 array) or 4% (type 2 array) if the photons are hitting the adjacent chamber. This low value indicates that the thickness of the ridges suffices to greatly reduce the transmission of secondary electrons across the ridge; the residual value of a few percent is due to the "side wings" of the scanned slit beam [Fig. 2(b)]. By scanning in both main directions (x and y) of the chambers of the array, identical signal profiles have been recorded. Furthermore, measurements carried out for various single chambers only showed negligible differences.

C. Construction of the two-dimensional response function

Due to its finite size and sensitivity to secondary electrons emerging from the ridges, each single chamber within the array is characterized by a two-dimensional response function $g(x,y)$, where x and y are the coordinates of a photon entering the array and (0,0) is the center of the chamber. From the signal profiles obtained by slit scanning in 1 mm steps (Fig. 5), we know that the one-dimensional response functions $f(x)$ and $f(y)$ have identical shapes. These functions can be normalized so that

$$\sum_x f(x) = \sum_y f(y) = 1, \tag{1}$$

where the sums are extended in 1 mm steps in the positive and negative x and y directions across one chamber up to the centers of the neighbor chambers. An estimate for $g(x,y)$ is obtained as the product

$$g(x,y) = f(x) \cdot f(y). \tag{2}$$

The function $g(x,y)$ is defined as a matrix on points with 1 mm distances in the x and y directions. Using Eqs. (1) and (2), we see that

$$\sum_y g(x,y) = f(x) \quad \text{and} \sum_x g(x,y) = f(y), \tag{3}$$

these relations show that the assumed function $g(x,y)$ complies with the results of one-dimensional scanning. Our results obtained by measuring the response function in the diagonal direction have confirmed that the matrix $g(x,y)$ is a suitable approximation of the real two-dimensional response function.

Since the measured signal profiles shown in Fig. 5, compared with the true response functions $f(x)$, were slightly broadened due to the influence of the finite slit width used in the scanning experiment [Fig. 2(b)], we have to assume that the true profiles of the response function are somewhat narrower. The need for taking this into account was only relevant for the 2D-ARRAY version 2 because of the smaller size of its single chambers. Guided by Fig. 5 (right panel), we adopted for version 2 response functions $f(x)$ and $f(y)$ of trapezoidal form with an upper width of 5 mm and a lower width of 9 mm.

As a test of the correctness of the determined response functions, the dose profile of a 10 cm $\times$ 10 cm photon field at 6 MV was measured by scanning with an energy-compensated Si diode (PTW TM 60008). Because of its small sensitive area of 1 mm $\times$ 1 mm, the diode represents the true dose profile with high resolution (Fig. 6). Through convolution of the result of the diode measurement with the response function $g(x,y)$, the dose profile expected in measurements with the 2D-ARRAY was calculated (dotted line), and the dose profile was measured with a single 2D-ARRAY chamber (filled circles). The consistency of the convolved true dose profile with the measured values of the 2D-

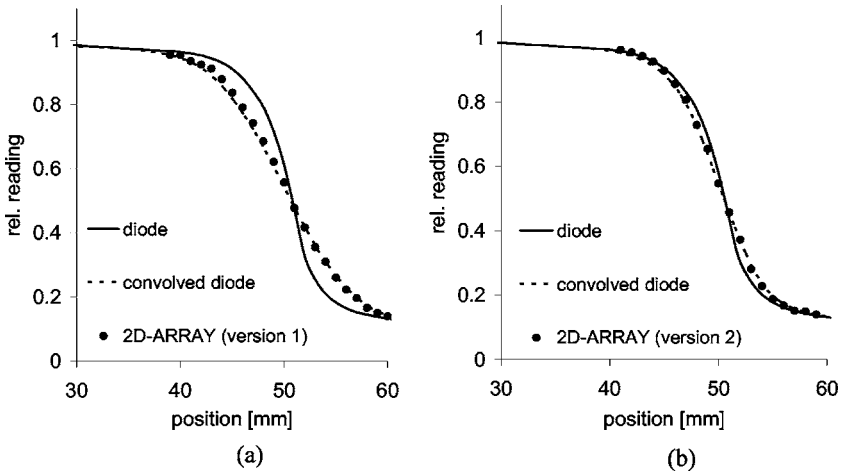

FIG. 6. Dose profile at the edge of a 10 cm × 10 cm photon field at 6 MV in the in-plane direction. A comparison of the true profile (diode values), the true profile convolved with the response function of the single chamber of the 2D-ARRAY, and the measured values of a single chamber of the 2D-ARRAY obtained by stepwise scanning across the dose distribution. (a) 2D-ARRAY version 1; (b) 2D-ARRAY version 2.

ARRAY single chamber demonstrates the correctness of the obtained response functions $g(x,y)$ for versions 1 and 2.

D. Performance of dosimetric plan verification

1. Basic concept

Based on the data in Fig. 6(b), one can conclude that the spatial resolution of the version 2 array can be regarded as sufficiently high to avoid any clinically relevant effect upon the measured dose profile, even if that profile comprises steep dose gradients. This has led to a practice of IMRT dose verification where TPS calculated dose profiles are directly compared to the measured set of version 2 sample values.[16,23] The application limits of this direct approach will be analyzed in the discussion. In the following, we are describing a more general strategy of dosimetric plan verification that has evolved in applications of the version 1 array, where the finite chamber size may cause slight, but noticeable differences between a given dose profile and the set of array sample values [compare Fig. 6(a)]. This approach is of general applicability for IMRT dose verifications with array detectors of non-negligible size.

Under consideration of the finite detector size, the basic concept for the verification of a given treatment plan is to calculate the two-dimensional matrix $E(x_i,y_j)$ of the *expected* readings at chamber positions x_i and y_j in the measurement plane of the 2D-ARRAY and to compare it with the matrix $M(x_i,y_j)$ of the *measured* values of the array. Acceptance criteria such as the gamma index[29] can then be applied. In order to allow for the volume effect[25] of the array chambers, the dose matrix $D(x,y)$, at a grid width of 1 mm, is convolved with $g(x,y)$, the two-dimensional response function of a single chamber. In this way the matrix $E(x,y)$ of the expected readings of the 2D-ARRAY

$$E(x,y) = D(x,y) * g(x,y), \tag{4}$$

is obtained. Values of $E(x_i,y_j)$ at the actual grid width of the chamber centers (x_i,y_j) are then used for comparison with the measured values of $M(x_i,y_j)$.

In the practical performance of this concept, a CT scan of the setup of the 2D-ARRAY at a depth of 10 cm within a 15 cm thick RW3 phantom was introduced into the TPS. The chamber's entrance plane was positioned at the isocenter distance (100 cm). For all subfields belonging to a given gantry angle, this angle was assumed to be 0°, and a common TPS calculation of matrix $D(x,y)$ was done for the horizontal 2D-ARRAY plane. The chosen field parameters were exported to our in-house record and verification system Herbie[27] for setting the irradiation parameters of the linear accelerator and calculating the values $E(x_i,y_i)$ according to Eq. (4). Through irradiation with the photon beam, the matrix of measured dose values $M(x_i,y_j)$ was obtained. Normalized matrix values $M^{\mathrm{norm}}(x_i,y_j)$ and $E^{\mathrm{norm}}(x_i,y_j)$ were used for further comparisons.

The flow chart of the comparison between measured and calculated two-dimensional dose distributions for a field of an IMRT plan is shown in Fig. 7 for a clinical example. The sequence consists of five subfields, with a smallest field size of 1 cm × 1 cm. The planned dose distribution, $D(x,y)$, calculated by the TPS, is convolved with $g(x,y)$, the two-dimensional lateral response function of a single array chamber. The resulting distribution of the expected readings at the positions of the chamber centers, $E^{\mathrm{norm}}(x_i,y_j)$, is then compared with the measured values of $M^{\mathrm{norm}}(x_i,y_j)$.

One might also think of deconvolving the measured values of the array chambers from the influence of $g(x,y)$ and comparing the result with the planned values $D(x,y)$. However, this is not possible in practice, because the matrix $M(x_i,y_j)$ of the measured values is only known at the grid width of the chamber centers, and because of other problems usually arising in deconvolutions.[31] For instance, if a deconvolution is performed using the convolution theorem, i.e. by dividing the Fourier transformation of the signal by the Fourier transform of the convolution kernel, noise in both of these functions may strongly affect the deconvolution result.

2. Correction of the array position

Special attention has to be paid to the positioning of the array. At the start of the verification measurements, the 2D-ARRAY is typically positioned by correlating, under visual control, the straight lines drawn on its surface with the laser

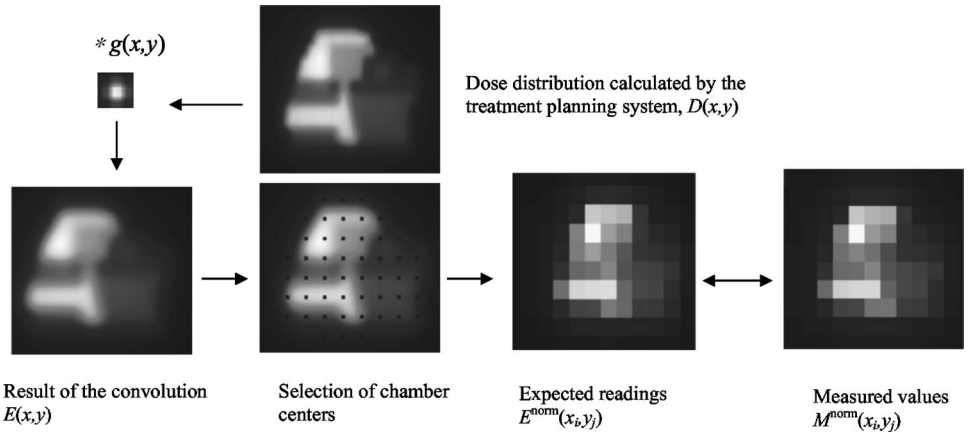

FIG. 7. Work flow chart of the comparison between expected and measured readings of the 2D-ARRAY. The procedure is shown for version 1 (type 10017).

beams of the therapy system. However, the accuracy that can be achieved by this method was found to be only approximately ±0.5 mm. A shift would possibly result in artificial dose differences between measurements and calculations, especially in high dose gradient regions. In order to avoid this effect, we introduced an algorithm to correct for any residual translation or rotation of the array with respect to the beam axis and the x and y directions of the accelerator head. For a standard open field of 10 cm × 10 cm at a depth of 10 cm in a 15 cm RW3 phantom, which was carefully centered in the laser beam system under visual control, the matrix $E^{\mathrm{norm}}(x_i,y_j)$ of the expected readings was compared to the measured values $M^{\mathrm{norm}}(x_i,y_j)$. As a global indicator for the shift and rotation of the array, we then calculated the sum of the squared differences between the expected and the measured values. Shifts and rotations were now varied within an interval of ±2 mm and ±1°. That combination that gave the minimum of the sum of squared differences was taken to indicate the true shift and rotation. Typical shifts were in the range of ±1 mm, and observable rotation errors did not occur. Further plan verification was then performed under the assumptionthat the position of the array had been accordingly corrected.

3. Examples of the comparison between expected and measured array readings

The process of the quantitative comparison can be illustrated by plotting the calculated plan data $D(x,y)$ of the TPS together with the expected readings $E^{\mathrm{norm}}(x_i,y_j)$ and the measured values $M^{\mathrm{norm}}(x_i,y_j)$ along a straight reference line, as shown for the version 1 array in Fig. 8. Although the expected and measured readings are strongly influenced by the existing high dose gradients in the in-plane direction of the accelerator, the measured values lie very close to the expected ones. To verify these results, film measurements have been carried out under isocentric conditions at the 2D-ARRAY's effective depth of measurement. The films were evaluated using a calibration curve obtained with a field size of 10 cm × 10 cm at the same depth-valid for the later dose profile measurement. The dose distribution obtained by film dosimetry is also shown in Fig. 8. This is a typical result with non-negligible differences between the unconvolved original plan data and the set of array sample values, which can be explained by the finite spatial resolution of the single chamber of the array.

Figure 8 has shown that chamber signals may be considerably influenced by high dose gradients. Therefore, we are applying the so-called gamma index introduced by Low *et al.*[29] as a mathematical method for the comparison of dose distributions in areas of high gradients. A measured value $M(x_i,y_j)$ at a point (x_i,y_j) will meet this criterion if at least one of the points representing the expected readings $E(x_k,y_l)$ is falling into an ellipse in the "feature space" of relative dose and coordinate differences, with half-axes of $\delta_{\max}$ and $\Delta_{\max}$ drawn around $M(x_i,y_j)$. Figure 9 illustrates the application of the gamma-index criterion. In the case of the typical

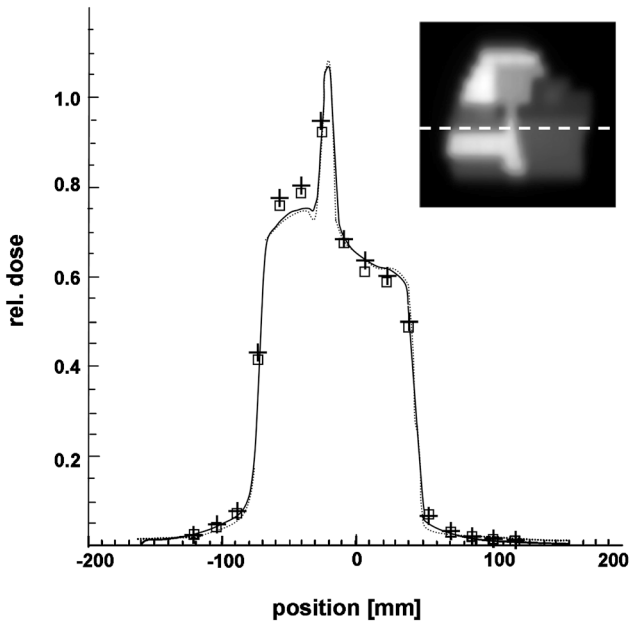

FIG. 8. Dose profile along the dashed line marked in the insert. Solid line: dose values $D(x,y)$ from planning system. Dotted line: profile from film measurement. Squares: expected readings $E^{\mathrm{norm}}(x_i,y_j)$ of the 2D-ARRAY (version 1). Crosses: measured values $M^{\mathrm{norm}}(x_i,y_j)$. The visible shift of the expected and measured readings from the profile is due to dose gradients in the direction vertical to the scanning line.

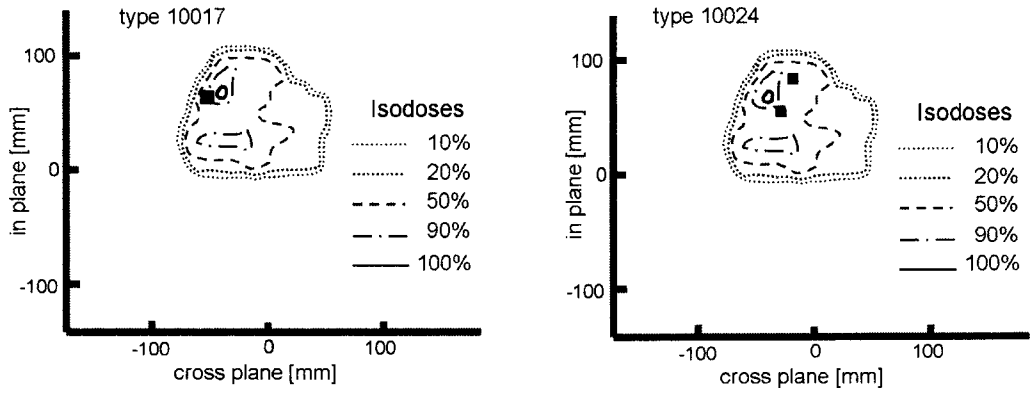

FIG. 9. Chamber readings failing the gamma-index criterion for the 2D-ARRAY's versions 1 and 2. Black squares: chambers failing the criterion with $\delta_{max}=3$ mm, $\Delta_{max}=3\%$. Lines: isodoses from the planning system.

values,[30] $\delta_{max}=3$ mm and $\Delta_{max}=3\%$, only one chamber of version 1 and two chambers of version 2 failed the criterion.

A case study for the error detection capabilities of the 2D-ARRAYs is illustrated in Fig. 10, which shows the effects of poorly positioned MLCs. In one segment of the sequence used in the former examples, an error was introduced artificially. The marked leaves were misaligned 2 mm to the right, compared to the reference sequence used in the examples above. In the corresponding chambers, the leaf errors resulted in a dose difference of 5% to 15%, as compared to the correct sequence. The figure illustrates the result when the expected and measured dose values were compared using a gamma index with $\delta_{max}=3$ mm and $\Delta_{max}=3\%$. In this example, all introduced errors have been detected by a failed gamma index.

IV. DISCUSSION

A. Air-filled detectors

A basic advantage of air-filled detectors is their insensitivity to radiation damage, also pointed out by Spezi *et al.*[23] With 2D-ARRAY versions 1 and 2 we have not detected any change in sensitivity exceeding ±1% over the whole period of use since 2001. Another advantage of air-filled detectors surrounded by materials of low atomic number is that they are free from any enhanced sensitivity to low-energy scattered photons due to the photoelectric effect in materials of the array. For the PTW 2D-Arrays, this has been illustrated by the achievement of the correct field-dependent output factors in this paper as well as in the experiments of Spezi *et al.*[23] and Wiezorek *et al.*[16] These observations also show that it is possible to calibrate the central chamber of the array by comparison with a reference-type thimble chamber. We have done this in 6 and 15 MV photon fields under IAEA reference conditions[35] and have obtained calibration factors close to those obtained by the manufacturer with Co-60 gamma radiation. However, for all measurements shown in this work, the analysis was done using normalized values.

B. Operational considerations

The strategy of using two-dimensional ionization chamber arrays to perform the dosimetric verification of IMRT fields serves to verify, in one single measurement, the sequence of all segments of the IMRT plan belonging to the same gantry angle. This is accomplished by setting the gantry angle to 0° with the 2D-ARRAY positioned in a phantom upon the irradiation table. While not all gantry directions can be analyzed in a single measurement, an eventually detected error can be directly related to the corresponding sequence of the plan. 2D arrays equipped with ionization chambers are typical for the necessity to deal with the influences of the detector size.

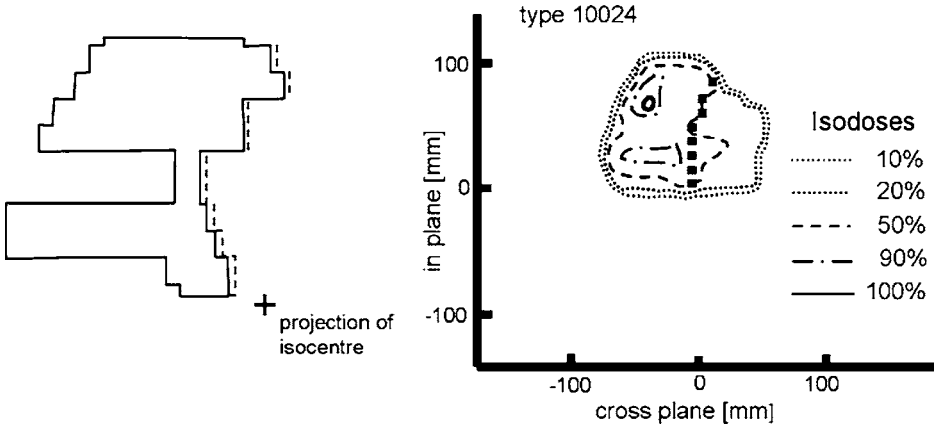

FIG. 10. Left: MLC shape of a segment of the IMRT field with introduced error. Solid line: segment without error. Dashed line: artificial MLC error of 2 mm. The relative weight of this segment to the overall field is 30%. Right: chambers failing to meet the gamma-index criterion after irradiation of the sequence (black square), with $\delta_{max}=3$ mm and $\Delta_{max}=3\%$. Lines: isodoses from a planning system (2D-ARRAY, version 2).

Spezi *et al.*[23] and Wiezorek *et al.*[16] performed dosimetric verifications by directly comparing the TPS calculated dose profile to the set of measured values of the 2D-ARRAY version 2. The suitability of this approach was demonstrated by the good agreement of the array values with those obtained with a small ionization chamber.[23,16] In terms of pattern analysis, the spatial frequency spectrum of the response function of the version 2 single chamber has its first zero near 1.4 cm^{-1}. Therefore, the simplified procedure applied by Spezi *et al.*[23] and Wiezorek *et al.*[16] is appropriate for version 2 applications when the spatial frequencies in the dose profile do not exceed 1.4 cm^{-1}.

In contrast to that, the convolution procedure described in this paper is typical for version 1 applications and can be generally applied in the case of single detectors of finite size. The first zero of the spatial frequency spectrum of a single chamber of the version 1 array is near 0.9 cm^{-1}. Therefore, the set of computed dose values is convolved with the response function of a single chamber of the array, and the expected chamber signals thereby obtained are then compared with the set of the measured array signals. This procedure is as well suited to perform dosimetric plan verifications; its principle is to avoid the occurrence of discrepancies due to the limited resolution of the single chamber by limiting the verification process to dose data that have already been weighted with the response function of the single chamber.

The examples that we studied showed that discrepancies mainly occurred at points with large dose gradients. If the consistency of expected and measured dose distributions is evaluated by the gamma-index criterion, most of the mentioned discrepancies disappear. Errors exceeding a typical gamma index with maximums of 3% dose deviation and 3 mm lateral deviation can be detected as long as they occur over the sensitive parts of a single chamber. Equivalent results have been found at higher photon energies.

C. Sampling step width

In a multi-detector array, the lateral dose distribution at the effective depth of measurement is sampled at the step width given by the distance between the single detectors. With regard to the resolution requirements of this sampling process, it is useful to consider that step-shaped fluence profiles in the photon beam are broadened by penumbra effects, and the absorbed dose profiles in the body or phantom are further broadened due to the emission of scattered photons and the emission, scattering and range of secondary electrons.[32] For example, according to film dosimetric measurements of the absorbed dose line-spread function at different depths,[10] the full 50% width of the line-spread function of a 6 MV photon beam is 9.7 mm at 4 mm PMMA depth and 11.6 mm at 50 mm PMMA depth, and the corresponding 50% widths for 15 MV are 12.0 and 16.5 mm [compare Fig. 2(b)]. This fundamental property of the clinically achievable dose profiles shows that in extreme cases there will be the need to resolve details having spatial frequencies up to 1 cm^{-1}, whereas weaker requirements may occur in many practical cases. In terms of the Nyquist theorem, this means that sampling frequencies up to 2 cm^{-1} may be required.

In case of the 2D-ARRAY, the user can choose between the more economical version 1 with a sampling frequency of 0.6 cm^{-1} or version 2 with 1 cm^{-1}, depending on the resolution needed in the department. In order to deal with IMRT sequences resulting in higher spatial frequencies, we have proposed to take a second set of measured values of each sequence after shifting the 2D-ARRAY version 2 by 5 mm in the x direction.[33] The same has been proposed by Spezi *et al.*[23] With this method, a sampling frequency of 2 cm^{-1} can be achieved in the x direction. A drawback of the version 1 array is the line-to-line distance of 16 mm. By contrast, version 2 has a line-to-line distance of 10 mm, so that each line can be exactly attributed to one MLC leaf pair if its width projected upon the isocenter plane is 1 cm.

D. Comparable devices

Amerio *et al.*[18] have presented the ImRT MatriXX, a two-dimensional detector array containing 1024 chambers arranged in a matrix of 32×32 chambers. The cylindrical ionization chambers (4.5 mm in diameter, 5 mm in height) have a center-to-center distance of 7.62 mm, which means a sampling frequency of 1.3 cm^{-1}. However, most commercially used MLCs for IMRT have a projected leaf width in the isocenter of 10 mm, so that no simple association of the MLC's leaves to the rows of detectors of this array can be achieved as long as the array is placed in the isocenter. What remains to be determined is the lateral response function of a single chamber of the ImRT MatriXX array, and this will depend on the thickness and material of the ridges between the chambers. The shorter sampling period of the electrometers of 20 ms, compared to 400 ms with the 2D-ARRAY, does not appear to be a practical advantage because the reset logic of the latter is working without dead time.

On the side of the semiconductor arrays, Jursinic *et al.*[15] and Wiezorek *et al.*[16] presented and studied a two-dimensional array (MapCHECK™, Sun Nuclear, Melbourne, FL) made of 445 n-type shielded diodes with 0.8 mm $\times$ 0.8 mm cross sections, arranged in a 22 cm $\times$ 22 cm array with variable spacing between the detectors. In the inner 10 cm $\times$ 10 cm area of the matrix, a pixel spacing of 7.07 mm is realized, corresponding to a sampling frequency of 1.4 cm^{-1}, while in the rest of the array the distances vary between 10 and 14.14 mm. In the absence of air-filled spaces, the small detector size leads to a narrow lateral response function with regard to the dose profile at the effective depth of measurement. Therefore, IMRT plan verification can be performed without the convolution step that we have described for the version 1 ionization chambers. An analysis can be done by comparing measured and calculated values in absolute dose or as normalized values. Measurements of the field-size-dependent output factor with this device were error-free.[16] As reported by the authors,[15] a sensitivity degradation of the n-type diodes of approximately 2% per 1000 Gy of total exposure can be expected. Shielded

silicon diodes are known for systematic errors in performing dosimetry in the electron buildup region of photon fields,[34] but the MapCHECK array is determined for measurements at 5 cm or deeper in a phantom. Moran *et al.*[17] presented an Active Flat Panel Dosimeter on a Si base. Again, a high spatial resolution is obtained with this device, but higher costs and detector aging have to be expected.

The system based on a Gd_2O_2S scintillation detector plate of 0.4 mm thickness, covered by a 1 mm copper plate, equipped with a CCD camera with 12 bit output (ImRT QA System, Wellhoefer-Scanditronics) has a virtual pixel width of 0.4×0.4 mm^2. However, an enhanced sensitivity of this system to low-energy scattered photons due to the photoelectric effect, leading to the impossibility to measure error-free field-size-dependent output factors, has been revealed.[16] Similarly, the idea to use image plates made from storage phosphors such as $BaFBr:Eu^{2+}$, is captivating since these detectors are frequently used in imaging diagnostics and provide high spatial resolution. However again here, significant errors will be introduced by the enhanced sensitivity to energy-degraded scattered photons.

So far, the standard method for verifying two-dimensional dose distributions has been film dosimetry. The advantages of this method are worldwide experience and a high spatial resolution. The drawbacks of film dosimetry, the dependence of film sensitivity on photon energy and dose rate, are small and generally well known.[7,10] However, all authors conclude that film dosimetry is a time- and material-consuming method that requires the continuous availability of a high-precision and stable chemical processing technique. Furthermore, there is the general tendency in radiology and radiotherapy to increasingly employ digital methods within the department. Therefore, film-processing machines may be kept in working condition for IMRT quality assurance only. Compared to film dosimetry, plan verification with the 2D-ARRAY has proven to be more time efficient because the analysis can be performed without any further calibration or scanning procedures. In addition, the results can be obtained "on the fly," which means that the numerical verification for one field can be performed while the next field is already being measured.

V. SUMMARY AND CONCLUSIONS

We have reported on our development of two-dimensional detector arrays for the dosimetric verification of IMRT radiation fields. Version 1 (PTW type 10017) consists of 16×16 single ionization chambers with 16 mm distances from center to center, and version 2 (PTW type 10024) contains 27×27 single chambers with a 10 mm center-to-center distance. If version 2 is arranged at the isocenter distance, each row of the matrix of ionization chambers exactly corresponds to one pair of opposing MLC leaves. The highest detectable spatial frequency that can be obtained with version 2 by taking two frames at positions differing by 5 mm in the x direction is 1 cm^{-1}. The transport of secondary electrons between the single chambers is blocked by ridges. The lateral response functions of the single chambers of both array versions were measured by slit-scanning experiments, which illustrated the influence of secondary electrons produced in the ridges and transported into the air-filled sensitive volumes. For a given lateral dose distribution, the signal profile of an array is equal to the dose profile in the entrance plane of the air-filled volumes convolved with the lateral response function of single chamber.

The two-dimensional ionization chamber array, together with the developed plan verification strategy, is a suitable and easy-to-handle quality assurance device for IMRT. A high sensitivity to errors in the dose distribution has been documented by a case study. Further studies will focus on the absolute dosimetric calibration of the array, as well as on the detailed examination of error detection capabilities. Future work will be required to clarify whether the 2D detector array methods are able to replace film dosimetry completely.

ACKNOWLEDGMENTS

The reliable and friendly cooperation of Dr. E. Schüle, M. Lapp, R. Kranzer, and B. Allgaier of the company PTW-Freiburg, Germany, over the years, is gratefully acknowledged. We thank our anonymous reviewers for their generous and manifold support in matters of this paper.

[a]Corresponding author: Bjoern Poppe, Medical Radiation Physics, Carl-von-Ossietzky University and Pius-Hospital, Georgstr. 12, 26121 Oldenburg, Germany. Electronic mail: bjoern.poppe@uni-oldenburg.de

[1]T. Bortfeld, A. L. Boyer, W. Schlegel, D. L. Kahler, and T. J. Waldron, "Realization and verification of three-dimensional conformal radiotherapy with modulated fields," Int. J. Radiat. Oncol., Biol., Phys. **30**, 899–908 (1999).

[2]C. S. Chui, M. F. Chan, E. Yorke, S. Spirou, and C. Ling, "Delivery of intensity-modulated radiation therapy with a conventional multileaf collimator: Comparison of dynamic and segmental methods," Med. Phys. **28**, 2441–2449 (2001).

[3]B. Rhein, P. Haering, J. Debus, and W. Schlegel, "Dosimetric verification of IMRT treatment plans at the German Cancer Center (in German)," Z. Med. Phys. **12**, 122–132 (2002).

[4]W. Schlegel and P. Kneschaurek, "Inverse radiation treatment planning (in German)," Strahlenther. Onkol. **175**, 197–207 (1999).

[5]S. Webb, *Intensity-Modulated Radiation Therapy* (IoP Publishing, Bristol, 2001).

[6]G. A. Ezzell, J. M. Galvin, D. Low, J. R. Palta, I. Rosen, M. B. Sharpe, P. Xia, Y. Xiao, L. Xing, and C. X. Yu, "Guidance document on delivery, treatment planning, and clinical implementation of IMRT: Report of the IMRT subcommittee of the AAPM radiation therapy committee," Med. Phys. **30**, 2089–2115 (2003).

[7]C. Martens, I. Claeys, C. De Wagter, and W. De Neve, "The value of radiographic film for the characterization of intensity-modulated beams," Phys. Med. Biol. **47**, 2221–2234 (2002).

[8]S. G. Ju, Y. C. Ahn, S. J. Huh, and I. J. Yeo, "Film dosimetry for intensity-modulated radiation therapy: Dosimetric evaluation," Med. Phys. **20**, 351–355 (2002).

[9]X. R. Zhu, P. A. Jursinic, D. F. Grimm, F. Lopez, J. J. Rownd, and M. T. Gillin, "Evaluation of Kodak EDR2 film for dose verification of intensity-modulated radiation therapy delivered by a static multileaf collimator," Med. Phys. **29**, 1687–1692 (2002).

[10]A. Djouguela, "Film dosimetry-physical aspects, working conditions and applications in modern radiotherapy," Master's thesis, University of Oldenburg, Germany, 2005.

[11]Y. De Deene, "Gel dosimetry for the dose verification of intensity modulated radiotherapy treatments," Z. Med. Phys. **12**, 77–87 (2002).

[12]G. S. Ibbott, M. J. Maryanski, P. J. Eastman, S. D. Holcomb, Y. Zhang, R. G. Avison, M. Sanders, and J. C. Gore, "Three-dimensional visualization and measurement of conformal dose distributions using magnetic resonance imaging of BANG polymer gel dosimeters," Int. J. Radiat. Oncol.,

Biol., Phys. **38**, 1097–1103 (1997).
[13]B. M. Hesse, L. Spies, and B. A. Groh, "Tomotherapeutic portal imaging for radiation treatment verification," Phys. Med. Biol. **43**, 3607–3616 (1998).
[14]R. J. Watts, "Evaluation of a diode detector array for use as a linear accelerator QC device," Med. Phys. **25**, 247–250 (1998).
[15]P. A. Jursinic and B. E. Nelms, "A 2-D diode array and analysis software for verification of intensity modulated radiation therapy delivery," Med. Phys. **30**, 870–879 (2003).
[16]T. Wiezorek, N. Banz, M. Schwedas, M. Scheithauer, H. Salz, D. Georg, and T. G. Wendt, "Dosimetric quality assurance for intensity modulated radiotherapy. Feasibility study for a filmless approach," Strahlenther. Onkol. **181**, 468–474 (2005).
[17]J. M. Moran, D. A. Roberts, T. S. Nurushev, L. E. Antonuk, Y. El-Mohri, and B. A. Fraass, "An active matrix flat panel dosimeter (AMFPD) for in-phantom dosimetric measurements," Med. Phys. **32**, 466–472 (2005).
[18]S. Amerio, A. Boriano, F. Bourhaleb, R. Cirio, M. Donetti, A. Fidanzio, E. Garelli, S. Giordanengo, E. Madon, F. Marchetto, U. Nastasi, C. Peroni, A. Piermattei, C. J. Sanz Freire, A. Sardo, and E. Trevisiol, "Dosimetric characterization of a large-area pixel-segmented ionization chamber," Med. Phys. **31**, 414–420 (2004).
[19]B. Poppe, R. Kollhoff, and A. Rubach, "First experiences with a two-dimensional ionization chamber (in German)," in *Medizinische Physik 2001*, edited by K. Welker and K. Zink, Berlin 2001, ISBN 3-89391-960-0, pp. 209–210.
[20]B. Poppe, P. Mehran, R. Kollhoff, and A. Rubach, "Use of a two-dimensional ionization-chamber array for quality assurance at medical linear accelerators (in German)," Z. Med. Phys. **13**, 115–122 (2003).
[21]B. Poppe, A. Blechschmidt, R. Kollhoff, A. Djouguela, A. Rubach, M. Lapp, E. Schüle, and D. Harder, "Lateral resolution of a new 2D ionization chamber array (in German)" in *Medizinische Physik 2003*, edited by W. Semmler and L. Schaad, Heidelberg, 2003, ISBN 3-925218-77-7, pp. 20–21.
[22]A. Djouguela, B. Poppe, R. Kollhoff, P. Mehran, and A. Rubach, "Introduction of a quality assurance program in radiation therapy with a two-dimensional ionization chamber array," in *Medizinische Physik 2003*, edited by W. Semmler and L. Schaad, Heidelberg, 2003, ISBN 3-925218-77-7, pp. 286–287.
[23]E. Spezi, A. Angelini, F. Romani, and A. Ferri, "Characterization of a 2-D ion chamber array for the verification of radiotherapy treatments," Phys. Med. Biol. **50**, 3361–3373 (2005).
[24]D. Harder, A. Rubach, K. P. Hermann, and A. Überschaer, "Water and tissue equivalent polystyrol phantoms for high energy photon and electron radiation (in German)," in *Medizinische Physik 1988*, edited by F. Nuesslin, Tuebingen, 1988, ISBN 3-925218-05-X.
[25]J. F. Dempsey, H. E. Romeijn, J. G. Li, and J. R. Palta, "A Fourier Analysis of the dose grid resolution required for accurate IMRT fluence map optimization," Med. Phys. **32**, 380–388 (2005).
[26]H. Kaminski and A. Rubach, "Development of a personal computer based record and verify system (in German)," in *Medizinische Physik 1996*, edited by H. Leitner and G. Stuecklschweiger, Graz, 1996, ISBN 3-925218-61-0, pp. 155–166.
[27]W. U. Laub and T. Wong, "The volume effect of detectors in the dosimetry of small fields used in IMRT," Med. Phys. **30**, 341–347 (2003).
[28]International Commission on Radiation Units and Measurements, "The dosimetry of pulsed radiation," ICRU Report 34, Bethesda, MD, 1982.
[29]D. Low, W. B. Harms, S. Mutic, and J. Purdy, "A technique for the quantitative evaluation of dose distributions," Med. Phys. **25**, 656–661 (1998).
[30]D. Low, "Physics of intensity modulated radiation therapy for head and neck cancer," in *Intensity Modulated Radiation Therapy for Head and Neck Cancer*, edited by K. S. Clifford Chao and G. Ozyigit (Lippincot, William and Wilkens, 2003), pp. 1–17.
[31]W. H. Press, S. A. Teukolsky, W. T. Vetterling, and B. P. Flannery, *Numerical Recipes in C: The Art of Scientific Computing* (Cambridge University Press, Cambridge, 1992).
[32]T. Bortfeld, U. Oelfke, and S. Nil, "What is the optimum leaf width of a multileaf collimator?," Med. Phys. **27**, 2494–2502 (2000).
[33]B. Poppe, A. Blechschmidt, A. Djouguela, R. Kollhoff, A. Rubach, and D. Harder, "High-resolution verification of IMRT plans using 2D-ARRAYs," Proceedings of the 2005 IOMP Conference, Nuremberg.
[34]I. Griessbach, M. Lapp, J. Bohsung, G. Gademann, and D. Harder, "Dosimetric characteristics of an unshielded silicon diode and its suitability for special applications in photon and electron beams," Med. Phys. **32**, 3750–3754 (2005).
[35]International Atomic Energy Agency, Vienna, "Absorbed dose determination in external beam radiotherapy," IAEA Technical Report Series No. 398, 2000).